Physics Letters B 728 (2014) 427–432

Contents lists available at ScienceDirect

Physics Letters B

www.elsevier.com/locate/physletb

Ginzburg–Landau phase diagram of QCD near chiral critical point – chiral defect lattice and solitonic pion condensate

Hiroaki Abuki

Department of Physics, Tokyo University of Science, Kagurazaka 1-3, Shinjuku, Tokyo 162-0825, Japan

ARTICLE INFO

Article history:
Received 20 September 2013
Accepted 18 November 2013
Available online 23 November 2013
Editor: J.-P. Blaizot

Keywords:
Chiral symmetry breaking
Charged pion condensate
Inhomogeneous condensates

ABSTRACT

We investigate the influence of the isospin asymmetry on the phase structure of quark matter near the chiral critical point systematically using a generalized version of Ginzburg–Landau approach. The effect has proven to be so profound that it brings about not only a shift of the critical point but also a rich variety of phases in its neighborhood. In particular, there shows up a phase with spatially varying charged pion condensate which we name the "solitonic pion condensate" in addition to the "chiral defect lattice" where the chiral condensate is partially destructed by periodic placements of two-dimensional wall-like defects. Our results suggest that there may be an island of solitonic pion condensate in the low temperature and high density side of QCD phase diagram.

1. Introduction

The chiral critical point (CP) in QCD phase diagram is the subject of extensive theoretical/experimental studies [1]. It was shown in [2,3] that once the possibility of inhomogeneity is taken into account, the CP turns into a Lifshitz critical point (LCP) where a line of the chiral crossover meets two lines of second-order phase transitions surrounding the phase of an inhomogeneous chiral condensate. The inhomogeneous state can be viewed as an ordered phase separation, produced via the compromise between quark–antiquark attraction and a pair breaking due to imbalanced population of quarks and antiquarks [4,5]. Such inhomogeneity appears rather commonly in a wide range of physics; the Abrikosov lattice [6] and the Fulde–Ferrell–Larkin–Ovchinnikov superconductors [7] are such examples.

In this Letter, we address the question what is the possible impact of the effect of an isospin asymmetry on the LCP. For bulk systems such as matter realized in compact stars, the flavor symmetry breaking is caused mainly by a neutrality constraint that should be imposed to prevent the diverging energy density. The effect leads to a rich variety of color superconducting phases at high density [8]. On the other hand, at large isospin density QCD vacuum develops a charged pion condensate (PC) as soon as $|\mu_{\rm I}| > m_\pi$ with m_π and $\mu_{\rm I}$ being the vacuum pion mass and the isospin chemical potential [9]. The PC has a rich physical content including a crossover from a Bose–Einstein condensate of pions to a superfluidity of the Bardeen–Cooper–Schrieffer type, and has been extensively studied using effective models [10].

We focus here how the neighborhood of CP is to be modified by inclusion of isospin density. To this aim, we use the generalized Ginzburg–Landau (GL) approach developed in [2,4] which can give rather model-independent predictions near the CP. Since we are interested in the response of the CP and its vicinity against $\mu_{\rm I} \neq 0$, our strategy is to take $\mu_{\rm I}$ as a perturbative field and expand the GL functional with respect to it. The inclusion of $\mu_{\rm I}$ further brings new GL parameters, but they can be evaluated within the quark loop approximation [2,4] since gluons are insensitive to isospin charge. What we will find is that the isospin asymmetry dramatically modifies the neighborhood of CP bringing about new multicritical points. Accordingly, an inhomogeneous version of charged pion condensate dominates a major part of phase diagram.

2. Generalized Ginzburg–Landau approach

We consider two-flavor QCD, and assume the existence of a tricritical point (TCP) in the (μ, T)-phase diagram in the chiral limit at vanishing $\mu_{\rm I}$. We take the chiral four vector $\phi = (\sigma, \boldsymbol{\pi}) \sim (\langle\bar{q}q\rangle, \langle\bar{q}i\gamma_5\boldsymbol{\tau}q\rangle)$ as a relevant order parameter of the system. A minimal GL description of TCP requires the expansion of the thermodynamic potential up to sixth order in ϕ. The resulting chiral O(4) invariant potential expanded up to the sixth order is, with incorporating the derivative terms as well [2,4]: $\omega[\phi(\mathbf{x})] = \sum_{n=1,2,3}\omega_{2n}[\phi(\mathbf{x})]$, where

$$\omega_2\big[\phi(\mathbf{x})\big] = \frac{\alpha_2}{2}\phi(\mathbf{x})^2, \quad \omega_4\big[\phi(\mathbf{x})\big] = \frac{\alpha_4}{4}\big(\phi^4 + (\nabla\phi)^2\big),$$

0370-2693
http://dx.doi.org/10.1016/j.physletb.2013.11.037

$$\omega_6[\phi(\mathbf{x})] = \frac{\alpha_6}{6}\Big(\phi^6 + 3\big[\phi^2(\nabla\phi)^2 - (\phi,\nabla\phi)^2\big] + 5(\phi,\nabla\phi)^2 + \frac{1}{2}(\Delta\phi)^2\Big). \tag{1}$$

The current quark mass adds to this a term $\omega_1[\sigma(\mathbf{x})] = -h\sigma(\mathbf{x})$ which explicitly breaks O(4) symmetry down to O(3), and thus makes the condensate align in the direction $\phi \to (\sigma, \mathbf{0})$. We use $\alpha_6^{-1/2}$ as a unit of an energy dimension. Accordingly we replace α_6 with 1, and every quantity is to be regarded as a dimensionless. Then via scaling $\phi \to \phi h^{1/5}$, $\mathbf{x} \to \mathbf{x}h^{-1/5}$ together with $\alpha_2 \to \alpha_2 h^{4/5}$, $\alpha_4 \to \alpha_4 h^{2/5}$, we can get rid of h in ω apart from a trivial overall scaling factor $h^{6/5}$, i.e., $\omega \to \omega h^{6/5}$. Then we set $h = 1$, and retain the original letters ϕ, $\mathbf{x}$, α_2, α_4 and ω hereafter, but we should keep in mind that they should scale as $h^{1/5}$, $h^{-1/5}$, $h^{4/5}$, $h^{2/5}$, $h^{6/5}$ respectively.

We assume that $\sigma(\mathbf{x})$ is spatially varying in one direction, z [2]. The Euler–Lagrange equation (EL), $\delta\omega/\delta\phi(z) = 0$, becomes

$$6h = \sigma^{(4)}(z) - 10\big(\sigma^2\sigma'' + \sigma(\sigma')^2\big) - 3\alpha_4\sigma'' + 6\sigma^5 + 6\alpha_4\sigma^3 + 6\alpha_2\sigma, \tag{2}$$

where h is temporarily recovered to remind us that the term comes from the mass term. We try the ansatz [3]

$$\sigma(z) = A\,\mathrm{sn}(kz - b/2, \nu)\mathrm{sn}(kz + b/2, \nu) + B, \tag{3}$$

where "sn" is the Jacobi elliptic function with ν the elliptic modulus, and k, b, A, B are real parameters. We call the state the "chiral defect lattice" (CDL).[1] This is a spatially modulating state having a period $\ell_p = 2K(\nu)/k$. Let us first show that the ansatz actually provides a one-parameter family of solution to the EL (2) when suitable conditions for A, B, k and b are met. First, we note from (3), $\mathrm{sn}(kz,\nu)^2 = \frac{(\sigma(z)-B)/A + b_2}{1+\nu b_2(\sigma(z)-B)/A}$ with $b_2 \equiv \mathrm{sn}(b/2,\nu)$. The fact that $f(z) = \mathrm{sn}(kz,\nu)$ obeys the Jacobi differential equation $(f')^2 = k^2(1-f^2)(1-\nu^2 f^2)$ translates into

$$d_0 = (\sigma')^2 + d_1\sigma + d_2\sigma^2 + d_3\sigma^3 + d_4\sigma^4, \tag{4}$$

where $\{d_0, d_1, d_2, d_3, d_4\}$ are functions of A, B, b, k and ν. We here give the expressions for d_3 and d_4 only,

$$d_3 = 4d_4\left(A\frac{\mathrm{cn}(b,\nu)\mathrm{dn}(b,\nu)}{\nu^2\mathrm{sn}^2(b,\nu)} - B\right), \quad d_4 = -\frac{k^2\nu^4\mathrm{sn}^2(b,\nu)}{A^2}. \tag{5}$$

Differentiating (4) with respect to z and dividing the result by $2\sigma'$, we obtain

$$-\frac{d_1}{2} = \sigma''(z) + d_2\sigma(z) + \frac{3d_3}{2}\sigma(z)^2 + 2d_4\sigma(z)^3. \tag{6}$$

Differentiating this twice we have

$$0 = \sigma^{(4)}(z) + 6d_4\sigma^2\sigma'' + 12d_4\sigma(\sigma')^2 + d_2\sigma'' + 3d_3(\sigma')^2 + 3d_3\sigma\sigma''. \tag{7}$$

Adding to this, $(f_0 + f_1\sigma(z))\times(4)$ and $(g_0 + g_1\sigma(z) + g_2\sigma(z)^2)\times(6)$ with f_0, f_1, g_0, g_1, g_2 being arbitrary constants, we obtain a wider fourth-order differential equation. Then by tuning $f_0 = g_1 = -3d_3$, we can get rid of unnecessary σ'^2 and $\sigma\sigma''$ terms, and setting $f_1 = -10 - 12d_4$, $g_2 = -10 - 6d_4$, $g_0 = -d_2 - 3\alpha_4$ leads to

$$\gamma(\{d_i\},\alpha_4) = \sigma^{(4)}(z) - 10\big(\sigma^2\sigma'' + \sigma(\sigma')^2\big) - 3\alpha_4\sigma'' - 6d_4(5+4d_4)\sigma^5 - 5d_3(5+6d_4)\sigma^4 + \sum_{n=3,2,1}\beta_n(\{d_i\},\alpha_4)\sigma^n, \tag{8}$$

where γ and β_n $(n = 1, 2, 3)$ are simple algebraic functions of d_0, d_1, d_2, d_3, d_4, and α_4. Matching the coefficients of σ^5 and σ^4 with those in (2) leaves two choices; $(d_3, d_4) = (0, -1)$ or $(0, -1/4)$. It turns out that the latter cannot satisfy the remaining constraints so we choose $(d_3, d_4) = (0, -1)$ which, with (5), constrains A and B as

$$A = k\nu^2\mathrm{sn}(b,\nu), \qquad B = k\frac{\mathrm{cn}(b,\nu)\mathrm{dn}(b,\nu)}{\mathrm{sn}(b,\nu)}. \tag{9}$$

The conditions $\beta_3 = 6\alpha_2$ and $\beta_2 = 0$ are then automatically satisfied, so we are left with two constraints $6h = \gamma$ and $6\alpha_2 = \beta_1$. Now that $\{d_i\}$ are functions of three variables $\{k, \nu, b\}$, the two conditions fix two of them, for instance, $\{k, b\}$ at a fixed elliptic modulus ν. Hence, the ansatz (3) together with (9) gives a one-parameter solution to (2). To our knowledge, this is the first demonstration of the fact that (3) constitutes a solution also in the GL functional approach which could be applied in a wide range of physics. The parameter ν is to be determined via the minimization of thermodynamic potential Ω, the spatial average of the energy density over one period $\ell_p = 2K(\nu)/k$:

$$\Omega(\nu;\alpha_2,\alpha_4) = \frac{1}{\ell_p}\int_{-\ell_p/2}^{\ell_p/2} dz\,\omega[\sigma(z)]. \tag{10}$$

Let us briefly check the two extreme limits, $\nu \to 1$ and $\nu \to 0$. First when $\nu \to 1$,

$$\sigma(z) \to \sigma_{\mathrm{sd}}(z) = \frac{k}{\mathrm{th}(b)}\big(1 - \mathrm{th}^2(b)\,f_{\mathrm{def.}}(kz,b)\big), \tag{11}$$

where the subscript "sd" refers to a "single-defect", and $f_{\mathrm{def.}}(kz,b) \equiv 1 - \mathrm{th}(kz+b/2)\mathrm{th}(kz-b/2)$. This describes a defect in chiral condensate, represented by a *soliton–antisoliton pair* located at $z = 0$. The homogeneous value gets eventually recovered as $|z| \to \infty$: $\sigma_{\mathrm{sd}}(\pm\infty) \equiv \sigma_L = k/\mathrm{th}(b)$. Since $k = \sigma_L\mathrm{th}(b)$, we regard $\sigma_{\mathrm{sd}}(z)$ as a function of z parametrized by σ_L and b. On the other hand, when $\nu \to 0$ the ansatz reduces to, retaining up to the first non-trivial order in ν,

$$\sigma(z) \to \sigma_{\sin}(z) = k\cot(b) - \nu^2\frac{k\sin(b)}{2}\cos(2kz). \tag{12}$$

This is the state where chiral condensate is about to develop a ripple sinusoidal wave on the homogeneous background. We denote the background chiral condensate as $k\cot(b) \equiv \sigma_S$, $\sigma_{\sin}(z)$ is now viewed as a function of z parametrized by σ_S, k, and vanishing ν.

3. Phase structure at $\mu_1 = 0$

We compute the phase diagram via minimization of (10). The result is displayed in Fig. 1. The CP is indeed realized as the LCP where the three phases meet; the CDL phase with $\sigma(z)$, the chiral symmetry broken (χSB) phase with a homogeneous condensate σ_L, and the nearly symmetry-restored phase characterized by a smaller condensate σ_S. For illustration, also shown by a solid line is the line of would-be first-order transition. Fig. 2 shows how $\sigma(z)$ smoothly interpolates between σ_L and σ_S along $\alpha_4 = -4$. Displayed in the left panel is the max amplitude $\max_z[\sigma(z)]$ as a function of α_2. Abrupt drop in σ indicated by a solid line shows the location of would-be first-order transition which would have

[1] The ansatz is called the "solitonic chiral condensate" in [3]. As we will see later, the state can be viewed as periodically placed wall-like defects of chiral condensate, so we use the term "CDL" here.

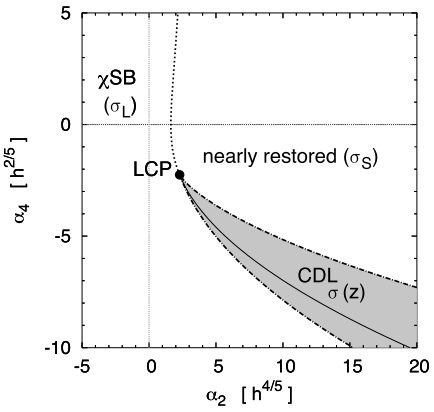

Fig. 1. The GL phase diagram at $\mu_{\rm I}=0$. The CDL is realized in the shaded region. The dotted line starting from the LCP $(\alpha_2^{\rm LCP},\alpha_4^{\rm LCP})\equiv(\frac{5}{4}\frac{3^{4/5}}{2^{2/5}},-\frac{5}{2^{1/5}3^{3/5}})$ stands for the crossover, while two dot-dashed lines enclosing the CDL denote the second-order phase transitions.

taken place if we ignored the possibility of inhomogeneity. Two figures in the right panel show the spatial profiles of $\sigma(z)$ for two values of α_2 denoted by **A** and **B**, whose locations are marked by a cross and a circle in the left figure. It looks like the periodic placements of defects near the σ_L-side, while it is just a tiny ripple sinusoidal wave near the σ_S-side. For both points, the σ_S-state exists as a local minimum, and its magnitude is depicted by a dot-dashed line. We see σ_S is roughly the median of $\sigma(z)$. At point **A**, the σ_L-state also exists as a metastable state. The magnitude of σ_L is shown by a dashed line, which roughly corresponds to the max amplitude of $\sigma(z)$. The modulation period, ℓ_p, is also shown by the arrow. ℓ_p grows towards the σ_L-side, evolving to infinity realizing a single defect state $\sigma_{\rm sd}(z)$ just at the onset.

Formation of a single defect. The second-order phase transition from the χSB phase to the CDL is signaled by the formation of a single wall-like defect (11), that is, a creation of soliton–antisoliton pair. Let us briefly describe this critical condition. When the defect forms in the sea of homogeneous background, mass per unit area associated with the wall extending in the transverse (x,y)-plane should vanish. The energy per unit area is $f_{\rm sd}(b;\alpha_2,\alpha_4)=\int_{-\infty}^{\infty}dz(\omega[\sigma_{\rm sd}(z)]-\omega[\sigma_L])$. Note that, for any (α_2,α_4), once the homogeneous value σ_L is numerically fixed, $f_{\rm sd}$ is a function of b only. In the left panel of Fig. 3, plotted are $f_{\rm sd}$ for $\alpha_2=3.5$, 3.76, 4.0 at $\alpha_4=-4$. We see that $\sigma_{\rm sd}(z)$ with $b\neq 0$ becomes more favorable once α_2 exceeds $3.76(\equiv\alpha_{2c})$, the critical value for defect formation onset. Note that the state with $b=0$ is equivalent to the χSB as $\sigma_{\rm sd}(z)\to\sigma_L$ with $b\to 0$ as seen from (11). In the right panel of Fig. 3, the spatial profile of $\sigma_{\rm sd}(z)$ at $\alpha_2=\alpha_{2c}$ is depicted by a light solid line, and that of energy density $\omega[\sigma_{\rm sd}(z)]-\omega[\sigma_L]$ is drawn by a heavy solid line. Contribution from each ω_i is also separately shown. We see that the gradient terms in particular in ω_6, and ω_2 are responsible for the spontaneous generation a defect.

Rippling of the chiral condensate. To derive the critical line separating the CDL and σ_S-phases, we first plug (12) into (10), then minimize the result over b and perform expansion about ν^2. Then looking at the location where the coefficient of ν^4 changes its sign, we reach the condition for the onset of rippling chiral condensate.

4. Phase structure for $\mu_{\rm I}\neq 0$

When we take $\mu_{\rm I}$ into consideration, the GL coefficients $\{\alpha_i\}$ become functions of $\mu_{\rm I}$, to be denoted by $\{\alpha_i(\mu_{\rm I})\}$. In addition, since $\mu_{\rm I}$ breaks the isospin $SU(2)_{\rm V}$ symmetry to $U(1)_{\rm I_3}$ which describes the rotation about the isospin third axis, the potential has new feedback terms which is invariant under $U(1)_{\rm I_3}$ but not under full $SU(2)_{\rm V}$. Up to the fourth order in $(\sigma,\boldsymbol{\pi})$, the most general form of the feedback potential describing the response to $\mu_{\rm I}$ is [11]

$$\delta\omega_{\rm I}=\frac{\beta_2}{2}\boldsymbol{\pi}_\perp^2+\frac{\beta_4}{4}\boldsymbol{\pi}_\perp^4+\frac{\beta_{4b}}{4}\big(\phi^2-\boldsymbol{\pi}_\perp^2\big)\boldsymbol{\pi}_\perp^2+\frac{\beta_{4c}}{4}(\nabla\boldsymbol{\pi}_\perp)^2,$$

where $\boldsymbol{\pi}_\perp=(\pi_1,\pi_2)$ is the charged pion doublet. When $|\boldsymbol{\pi}_\perp|\neq 0$, the residual $U(1)_{\rm I_3}$ (or equivalently the electromagnetic $U(1)_{\rm Q}$) gets broken spontaneously.

In order to find an expression of the potential up to the sixth order in $\{\mu_{\rm I},\sigma,\pi,\nabla\}$ we need to expand α_{2n}, β_2 and $\beta_{4,4b,4c}$ up to the corresponding orders in $\mu_{\rm I}$. Via explicit computations [11], we have $\alpha_6(\mu_{\rm I})=\alpha_6+\mathcal{O}(\mu_{\rm I}^2)$, $\alpha_4(\mu_{\rm I})=\alpha_4+\mu_{\rm I}^2\alpha_6+\mathcal{O}(\mu_{\rm I}^4)$ and $\alpha_2(\mu_{\rm I})=\alpha_2+\mathcal{O}(\mu_{\rm I}^6)$. β_2 and $\beta_{4,4b,4c}$ have the following general structure:

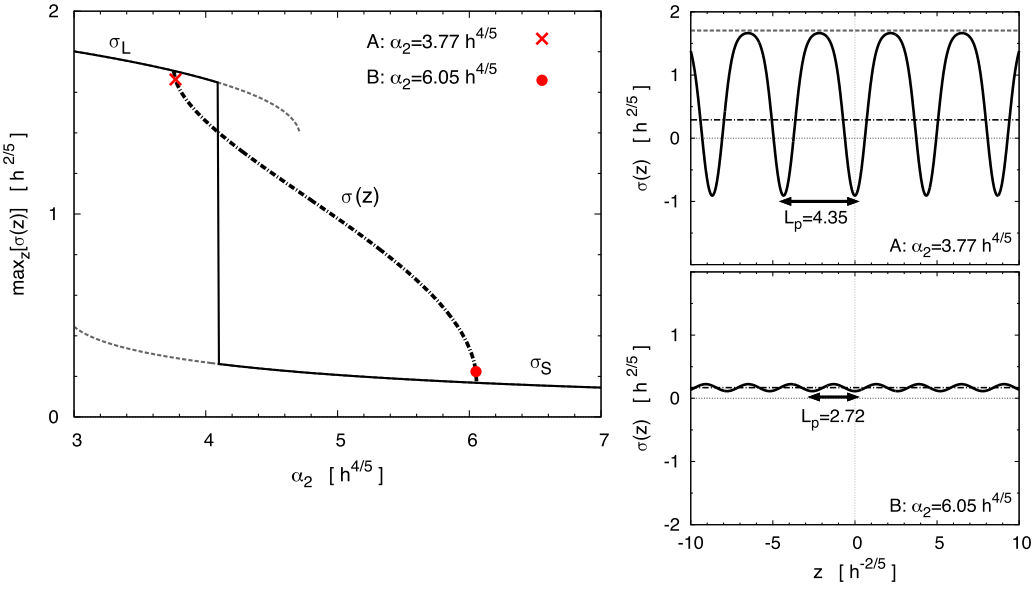

Fig. 2. (Left panel): The amplitude $\max_z[\sigma(z)]$ as a function of α_2 along the line $\alpha_4=-4$. (Right panel): The spatial profiles of $\sigma(z)$ at point **A** $(\alpha_2=3.77h^{4/5})$ and **B** $(\alpha_2=6.05h^{4/5})$ shown in the left figure by a cross and a circle.

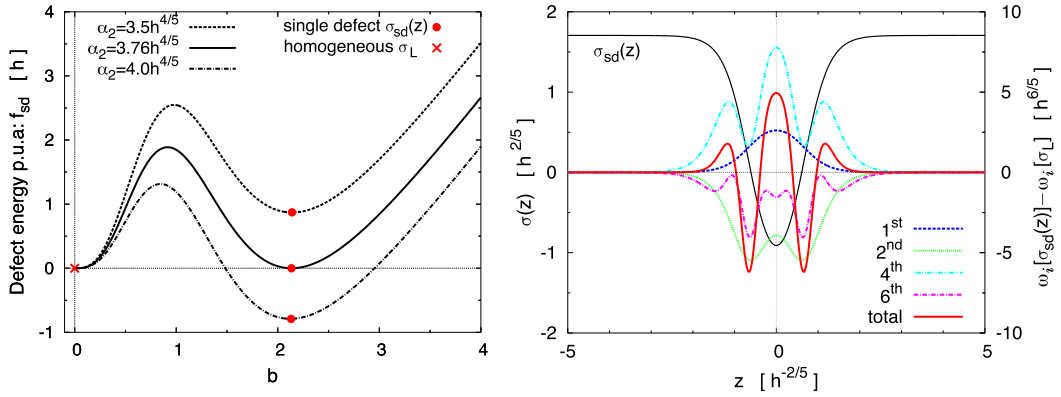

Fig. 3. (Left): The energy per unit area associated with a single wall-like defect as a function of b. (Right): The spatial profile of $\sigma_{\rm sd}(z)$ and energy density at the onset $\alpha_2 = 3.76h^{4/5}$.

$$\begin{pmatrix} \beta_2(\mu_{\rm I}) \\ \beta_{\{4,4b,4c\}}(\mu_{\rm I}) \end{pmatrix} = \mu_{\rm I}^2 \begin{pmatrix} a & e\mu_{\rm I}^2 \\ 0 & \{b,c,d\} \end{pmatrix} \begin{pmatrix} \alpha_4 \\ \alpha_6 \end{pmatrix} + \begin{pmatrix} \mathcal{O}(\mu_{\rm I}^6) \\ \mathcal{O}(\mu_{\rm I}^4) \end{pmatrix}.$$

Straightforward (but tedious) work leads to $a = -\frac{1}{2}$, $e = 0$, and $\{b,c,d\} = \{-2,-2,-\frac{4}{3}\}$. Plugging all these expressions into the potential $\omega + \delta\omega_{\rm I} \equiv \omega_{\rm t}$ we have

$$\begin{aligned}\omega_{\rm t} = {}& \omega_6\big[\phi(\mathbf{x})\big] - h\sigma + \frac{\alpha_2}{2}\sigma^2 + \left(\frac{\alpha_2}{2} - \frac{\mu_{\rm I}^2\alpha_4}{4}\right)\boldsymbol{\pi}_\perp^2 \\ & + \left(\frac{\alpha_4}{4} + \frac{\mu_{\rm I}^2\alpha_6}{4}\right)\sigma^4 + \frac{\alpha_4}{2}\sigma^2\boldsymbol{\pi}_\perp^2 + \left(\frac{\alpha_4}{4} - \frac{\mu_{\rm I}^2\alpha_6}{12}\right)\boldsymbol{\pi}_\perp^4 \\ & + \left(\frac{\alpha_4}{4} + \frac{\mu_{\rm I}^2\alpha_6}{4}\right)(\nabla\sigma)^2 + \left(\frac{\alpha_4}{4} - \frac{\mu_{\rm I}^2\alpha_6}{12}\right)(\nabla\boldsymbol{\pi}_\perp)^2. \qquad (13)\end{aligned}$$

We see that h favors condensation in the σ-direction, while $\mu_{\rm I}$ prefers $\boldsymbol{\pi}_\perp \neq 0$. Now the potential has parameters $\{\alpha_2, \alpha_4, \alpha_6, h\}$ and $\mu_{\rm I}^2$. Repeating the same dimensional and scaling analysis as before, we get rid of α_6 and h, so the remaining parameters are α_2, α_4 and $\mu_{\rm I}^2$ which scale as $h^{4/5}$, $h^{2/5}$ and $h^{2/5}$.

The remaining task is to find the most favorable state for a given parameter set of $\{\alpha_2, \alpha_4, \mu_{\rm I}^2\}$. We here consider four variational states:

(i) The χSB state with $\sigma \neq 0$, $\boldsymbol{\pi}_\perp = 0$.
(ii) The CDL state with $\boldsymbol{\pi}_\perp = 0$, $\sigma(z)$ described in (3). In the same way as before, with a replacement $\alpha_4 \to \alpha_4 + \mu_{\rm I}^2$ we can show this gives a solution to the EL.
(iii) The homogeneous charged pion condensate (PC) with $\boldsymbol{\pi}_\perp = (\pi, 0)$, $\sigma \neq 0$.
(iv) The solitonic charged pion condensate (SPC) with

$$\sigma \neq 0, \quad \boldsymbol{\pi}_\perp = \big(\pi(z), 0\big), \quad \pi(z) = k\nu\,\mathrm{sn}(kz, \nu).$$

This indeed gives a solution to the EL.

In Table 1, we summarize these states with associated symmetries.[2]

In Fig. 4 we display the GL phase diagrams computed for $\mu_{\rm I}^2 = 0.01$ (a), 0.1 (b), 0.2 (c), and 0.5 (d). Let us start with the case $\mu_{\rm I}^2 = 0.01$. First, a rough order estimate is useful to have in mind what is the physical scale of $\mu_{\rm I}$. Since $h \sim m_q/\Lambda$ with $m_q \sim 10$ MeV and $\Lambda \sim 1$ GeV being the current quark mass and

Table 1
State candidates for $\mu_{\rm I} \neq 0$.

	σ	$\pi_\perp$	Internal symmetry	Translation
χSB	$\sigma \neq 0$	$\pi_\perp = 0$	$\mathrm{U(1)_B \times U(1)_Q}$	Unbroken
PC	$\sigma \neq 0$	$\pi \neq 0$	$\mathrm{U(1)_B}$	Unbroken
CDL	$\sigma(z)$	$\pi_\perp = 0$	$\mathrm{U(1)_B \times U(1)_Q}$	Broken
SPC	$\sigma \neq 0$	$\pi(z)$	$\mathrm{U(1)_B}$	Broken

the energy scale for chiral symmetry breaking, $\mu_{\rm I}^2 = 0.01$ corresponds to $\mu_{\rm I} = 0.1\Lambda(m_q/\Lambda)^{1/5} \sim 40$ MeV. We see that the LCP found in the previous analysis is intact apart from the trivial shift of its location $(\alpha_2^{\rm LCP}, \alpha_4^{\rm LCP}) \to (\alpha_2^{\rm LCP}, \alpha_4^{\rm LCP} - \mu_{\rm I}^2)$, which is absorbed in the redefinition of the vertical axis: $\alpha_4 \to \alpha_4 + \mu_{\rm I}^2$. The major topological change from the case $\mu_{\rm I} = 0$ is the appearance of an island for the SPC replacing a part of the CDL phase which would have extended off the LCP. In fact, the second-order transition from the σ_S-phase to the CDL is taken over by the one to the SPC for $\alpha_4 \lesssim -6.16$ where the instability for developing an infinitesimal sinusoidal density wave of the charged pion condensate takes place earlier than that for rippling the chiral condensate. This is because $\mu_{\rm I}^2$ makes the coefficient of negative gradient term $(\pi_\perp')^2$ larger than that of $(\sigma')^2$ by $\mu_{\rm I}^2\alpha_6/3$ as seen in (13). On the other hand, the SPC and CDL phases are separated by a first-order transition. As a consequence, there is a bicritical point marked by "BCP" where a first-order transition meets two second-order transitions.

Let us briefly discuss what can be a possible interpretation of the physical reason why an inhomogeneous pion condensate occurs at large value of α_2 which roughly corresponds to the high density side of the (μ, T)-phase diagram [11]. The pion condensate for $\mu_{\rm I} > 0$ is described by the formation of u and $\bar{d}$ quark pair on the matched Fermi surface $\mu_{\rm I}$ [9]. The effect of μ is to break the pair making mismatched Fermi surface via producing a net excess of u quarks to $\bar{d}$ quarks. When this effect stresses the pair condensate, it is sometimes possible that the pairing is partially broken periodically in the real space or the momentum space such as in the FFLO superconductor in the presence of an external magnetic field [7].

When $\mu_{\rm I}^2$ increases to 0.1, the situation changes to the one displayed in Fig. 4(b). The CDL region shrinks and the SPC now occupies a major part. The transition between the SPC and χSB phases is first-order, accompanied by an abrupt change in σ. Accordingly there shows up point "E" at which a second-order transition comes across two first-order transitions. Another notable change is the appearance of continent of PC in the deep inside the χSB phase [11]; the two phases are separated by a second-order transition. Fig. 4(c) shows the situation for $\mu_{\rm I}^2 = 0.2$. The PC now meets the SPC island, and their competition gives rise

[2] We also tried two other exotic inhomogeneous states. One is the "skewed chiral spiral" defined by $\sigma = \sigma_0 + A\sin(kz)$, and $\pi_1 = B\cos(kz)$, which is an extension of the "CDW" introduced in [12], and the other is the "IPC" state taken in [13]. These were found to be less favorable than the CDL (or SPC) state for any value of $\mu_{\rm I}$.

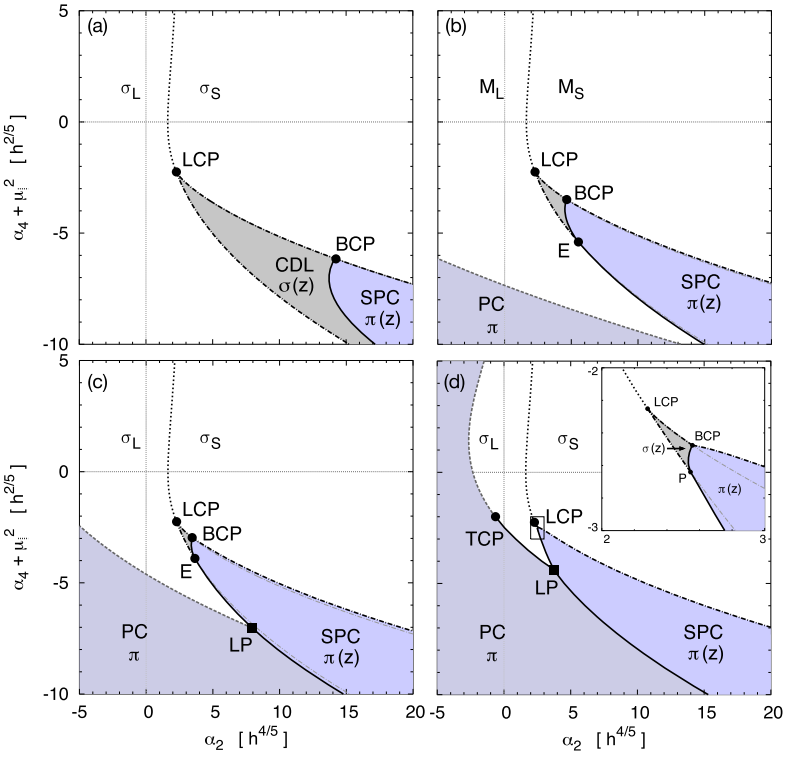

Fig. 4. The GL phase diagram for $\mu_1^2 = 0.01$ (a), 0.1 (b), 0.2 (c) and 0.5 (c). The solid lines stand for first-order phase transitions, while (dot-)dashed lines represent second-order phase transitions.

to a first-order phase boundary between them. As a result there appears a new Lifshitz point "LP", which has two branches of first-order transitions, and a second-order transition between the PC and χSB phases. The phase diagram for $\mu_1^2 = 0.5$ is shown in Fig. 4(d). The CDL region shrinks so much that its existence can be only confirmed in the inset figure that magnifies the vicinity of the LCP. The transition between the PC and χSB phases changes to first-order before coming across the SPC island. As a result, the LP now has three branches of first-order transitions.

5. Conclusion

We investigated systematically the two-flavor QCD phase diagram near the CP using a generalized version of GL approach, combined with the perturbative expansion in μ_1. We have clarified that the effect of isospin imbalance brings about drastic changes in the phase structure. The most significant one is the stabilization of the SPC for a wide range of GL parameter space. Our results suggest that at low temperature, going down in density from high density side, one may have a second-order phase transition from the nearly chirally symmetric matter to the SPC, which is signaled by development of a ripple sinusoidal density wave of a charged pion condensate. The state eventually evolves to solitonic lattice.

The magnetic property of inhomogeneous pion condensate is worth to be addressed in the future. The homogeneous PC has an electric charge, so is also a superconductor. Thus it should exhibit a Meissner effect by which a weak magnetic field applied to the system is expelled from the bulk. In the inhomogeneous SPC phase, however, there are domainwalls where the pair is effectively broken so that the magnetic field can penetrate there. This may bring some phenomenological consequences to compact star physics.

There remain a couple of interesting questions unsolved. First, it would be interesting to explore the possibility of higher dimensional lattice structures. In particular it may be possible that the three-dimensional spherical chiral defect is formed in advance of the two-dimensional wall-like defect studied here. Second, it is interesting to specify the low energy excitations on the SPC/CDL and clarify their nature. Lastly, it should be worth trying to extend the current GL analyses to three-flavor case where we have to take care a possible Kaon condensate driven by the chemical potential for strangeness. The future study along these directions would be the first step towards clarifying how these exotic inhomogeneous states leave unique footprints in the phenomenology of compact star physics.

Acknowledgements

The author thanks M. Ruggieri for several useful comments. Numerical calculations were carried out on SR16000 at YITP in Kyoto University.

References

[1] See for an extensive review, K. Fukushima, T. Hatsuda, Rep. Prog. Phys. 74 (2011) 014001.
[2] D. Nickel, Phys. Rev. Lett. 103 (2009) 072301.
[3] D. Nickel, Phys. Rev. D 80 (2009) 074025.
[4] H. Abuki, D. Ishibashi, K. Suzuki, Phys. Rev. D 85 (2012) 074002.
[5] K. Fukushima, Phys. Rev. D 86 (2012) 054002.
[6] A.A. Abrikosov, J. Explt. Theoret. Phys. (USSR) 32 (1957) 1147.
[7] P. Fulde, R.A. Ferrell, Phys. Rev. 135 (1964) A550;
A. Larkin, Y. Ovchinnikov, Zh. Eksp. Teor. Fiz. 47 (1964) 1136;
A. Larkin, Y. Ovchinnikov, Sov. Phys. JETP 20 (1965) 762.
[8] See, for example, K. Iida, T. Matsuura, M. Tachibana, T. Hatsuda, Phys. Rev. Lett. 93 (2004) 132001;
H. Abuki, M. Kitazawa, T. Kunihiro, Phys. Lett. B 615 (2005) 102;
H. Abuki, T. Kunihiro, Nucl. Phys. A 768 (2006) 118.
[9] D.T. Son, M.A. Stephanov, Phys. Rev. Lett. 86 (2001) 592.
[10] L.-y. He, M. Jin, P.-f. Zhuang, Phys. Rev. D 71 (2005) 116001;
L.-y. He, M. Jin, P.-f. Zhuang, Phys. Rev. D 74 (2006) 036005;
A. Barducci, R. Casalbuoni, G. Pettini, L. Ravagli, Phys. Rev. D 69 (2004) 096004;
J.O. Andersen, L. Kyllingstad, J. Phys. G 37 (2010) 015003;
H. Abuki, R. Anglani, R. Gatto, M. Pellicoro, M. Ruggieri, Phys. Rev. D 79 (2009) 034032;

for general thermodynamic structures of a relativistic crossover from fermion Cooper pairs to Bose superfluidity, see Y. Nishida, H. Abuki, Phys. Rev. D 72 (2005) 096004;
H. Abuki, Nucl. Phys. A 791 (2007) 117.
[11] H. Abuki, Phys. Rev. D 87 (2013) 094006;
Y. Iwata, H. Abuki, K. Suzuki, arXiv:1206.2870;
Y. Iwata, H. Abuki, K. Suzuki, AIP Conf. Proc. 1492 (2012) 293.
[12] E. Nakano, T. Tatsumi, Phys. Rev. D 71 (2005) 114006.
[13] N.V. Gubina, K.G. Klimenko, S.G. Kurbanov, V.C. Zhukovsky, Phys. Rev. D 86 (2012) 085011.